Available online at http://journal-of-agroalimentary.ro

Journal of Agro-alimentary Processes and Technologies 2024, 30 (2), 129-135

Journal of Agroalimentary Processes and Technologies

Hybrid pero vskite/polymer material. Preparation and physicochemical properties

Nick Samuel Țolea[1], Adina Căta[1], Antonina Lazăr[1], Ioana M.C. Ienașcu[1,2], Paula Svera[1], Daniel Ursu[1], Corina Orha[1], Paula Sfîrloagă[1,3*]

[1]National Institute of Research and Development for Electrochemistry and Condensed Matter, Dr. A. P. Podeanu 144, 300569, Timişoara, Romania
[2]"Vasile Goldiş" Western University of Arad, Faculty of Pharmacy, Liviu Rebreanu 86, 310045, Arad, Romania
[3]Spin-off Nattive-Senz SRL,Dr. A.P. Podeanu street, No. 144, 300569, Timisoara, Timis, Romania

**Corresponding author: paulasfirloaga@gmail.com*

Abstract
Organic–inorganic hybrid perovskites are a promising class of processable semiconducting materials that combine the favorable properties of the inorganic semiconductor with the flexibility and low-temperature processability of the organic material.Here, we report on the synthesis and investigation of the properties of a novel polymer-perovskite nanoparticles system based on LaMnO3:Ag nanocrystals protected by sodium polyacrylate polymer (PANa). The hybrid material was investigated by various characterization techniques, i.e. X-ray diffraction, FT-IR, RAMAN spectroscopyand SEM/EDAX. This type of sensor could meet the humidity detection needs and to assure the food safety.
Keywords: perovskite, polymer, hybrid

1. Introduction

Compounds with perovskite structure are promising materials in the field of current science and technology, matching the characteristics of photocatalytic processes, due to their stability, low costs of synthesis, high absorption properties, easy carrier recombination and mobility, optimum molar extinction coefficient and absorption in the visible spectrum [1]. Furthermore, perovskites are appreciated their diffusion length and prolonged charge carrier lifetime [2].

Perovskites have usually a cubic crystal structure designated by an ABX_3 system, where A is a cation larger in size than the B cation. A cation can be an inorganic compound such as metals, alkalis, lanthanides or rare earth metals or an organic compound such as methyl ammonium. On the other hand, B cation may consist in a transition metal ion and X is frequently represented by oxygen anion [3,4].

The modulation of the material properties can be achieved by using different possible combinations between the two cations, A and B, so that the properties of the obtained materials will perfectly fit the proposed applications. Besides many other applications of perovskite materials, worth mentioning are solar cells [5], light-emitting diode (LED) [6], X-ray imaging [7], and photocatalysts [3,8].

Still, the perovskites performance in practical application depends on their chemical and photochemical stability on

10.59463/JAPT.2024.2.07

environmental conditions (moisture, oxygen, and heat), which can be improved by combining with additional materials or by using encapsulation techniques. The role of polymers has been extensively researched as an alternative method in this regard [9,10]. So, due to the susceptibility of perovskites to moisture, many approaches have been conducted to improve the stability of perovskites, for instance, the film coating of perovskites with a layer of polymer effectively worked as a moisture barrier increasing the resistance to solvents and the tensile strength [11].

Thus, the polymers can protect the inorganic framework of the perovskites and add enhanced structural stability of the perovskites preventing defect formation or perovskite phase transitions. Moreover, the benefits of using polymers to improve electrical and optical properties of perovskites consist in improved charge transport, reduced trap states, and increased chemical reaction surface area [12].

regard, several researches have been carried out on the development of humidity detection sensors, like resistive [22,23], capacitive [24,25], impedance [26], optical [27] and mass sensitive [28] type, and materials such as metal oxides, sulphides, and carbon materials [29-32] were employed. Despite of the improvement in humidity detection, these materials are still unable to meet the detection needs.

Based on the excellent adsorption, hydrophilicity, natural availability, and outstanding film- forming properties, some polymers gained attention in this field. Superabsorbent polymers are hydrogels that can absorb many hundred times their own weight in water, and the most common one is sodium polyacrylate (NaPA). NaPA is known for its swelling behaviour during absorption [33] and for its resistance to solvents and high tensile strength forming a moisture barrier [11], so its application in various fields, such as anti-flood measures, water-retentive soil modifiers and soft actuators, were demonstrated [33].

For example, a rapid response humidity sensor based on gel polymer electrolyte MPOSS-PIL was developed. The sensor stability under high humidity environments can be related to the structure of the polymer interconnection network [34].

Hence, polymers have been investigated as additives to improve the efficacy and robustness of photocatalysts based on perovskite materials. There are many procedures used to incorporate polymers into perovskite structures, such as polymer coatings [13], in situ polymerization [14], spin-coating [15], electrospinning [16].

Recently, hybrid perovskite–polymer materials demonstrated excellent advances in the film morphology, device efficiency, and functioning stability of electronic devices [17-20]. Moreover, novel hybrid structures, polyvinylpyrrolidone functionalized with Ag-doped $LaMnO_3$ and Pd-doped $LaMnO_3$, respectively, were obtained and tested as good water electrolysis catalysts proving the role of polymers on the performance enhancement of the perovskite oxides in the water-splitting field [21].

Moreover, humidity is crucial to food safety, so, the effective detection of humidity is vital. In this

Moreover, Ponzoni et. al. explored the electrostatic stabilization of $BiFeO_3$ using NaPA as suspending agent and observed that the $BiFeO_3$ films used for photocatalytic applications showed efficient activity in the degradation of organic compounds both when used in the green state or after sintering [35]. Zhang et. al. proved the stability of the inverse microemulsion droplets of $Bi2WO_6$-sodium polyacrylate latex particles and the their strong ultraviolet-visible absorption characteristics and luminescence intensity [36].

The current research dealt with the preparation of a novel hybrid polymer-perovskite nanoparticles system based on $LaMnO_3$:Ag nanocrystals protected by sodium polyacrylate polymer (NaPA). The hybrid material was investigated by specific characterization techniques that demonstrated the proposed structure and offered a complete characterization of the material in terms of the surface morphology, and dimension of the crystals. The advent of high-performance solid-state gas sensors has motivated several scientists in searching the new perovskite materials or organic-inorganic hybrid materials based on perovskites and investigating their gas sensing properties.

2. Materials and Methods

2.1. Synthesis of Hybrid Materials

Perovskite material (1% Ag-doped $LaMnO_3$) obtained by a previously reported sol-gel technique [37] and sodium polyacrylate (Sigma-Aldrich) were used in the study for the synthesis of the hybrid material. The method of wet trituration at ambient temperature was used for the synthesis of hybrid material based on sodium polyacrylate ($C_3H_3NaO_2$) n and a perovskite structure of the $LaMnO_3$:Ag type. The mixture of $LaMnO_3$:Ag and sodium polyacrylate (1:20, w/w) was wet-triturated for 30 minutes, using distilled water, until hydrogels were obtained. The resulting hydrogels were dried at 60 °C for 12 h and then mortared until obtaining a powder with particle dimensions up to 1 mm. Finally, the powder was subjected to another drying stage at 60 °C for 4 h.

2.2. Characterization of Hybrid Materials

X-ray diffraction (XRD) data were collected using an X'Pert PRO MPD diffractometer (PANalytical, The Netherlands) with Cu-Kα radiation in the 2θ range of 10–80°. The FT-IR spectra were recorded at room temperature in the 4000–600 cm−1 range using a Bruker Vertex 70 spectrometer (Bruker Optik GmbH, Germany) equipped with a Platinium ATR unit, Bruker Diamond A225/Q.1. The morphology of the samples was registered using a scanning electron microscope equipped with energy dispersive X-ray detector (Inspect S, FEI Company Netherlands). Raman spectra were obtained with Shamrock 500i Spectrograph (Andor, United Kingdom) at room temperature using 514 nm laser excitation.

3. Results and Discussion

3.1. XRD Analysis

The structural analysis of organic-inorganic hybrid materials based on Ag-doped lanthanum manganite - functionalized with sodium polyacrylate, performed by X-ray diffraction, is presented in Figure 1.The structural characterization for the hybrid samples was achieved by powder X-ray diffraction (XRD) using a PANalyticalX′Pert Pro MPD-type diffractometer with Cu-Kα radiation (λCu= 1.54060 Å). The diffraction angle (2Theta) ranged between 10° and 80° and a 2θ-step of 0.2°/min. From the presented spectra it can be seen that the samples are well crystallized.

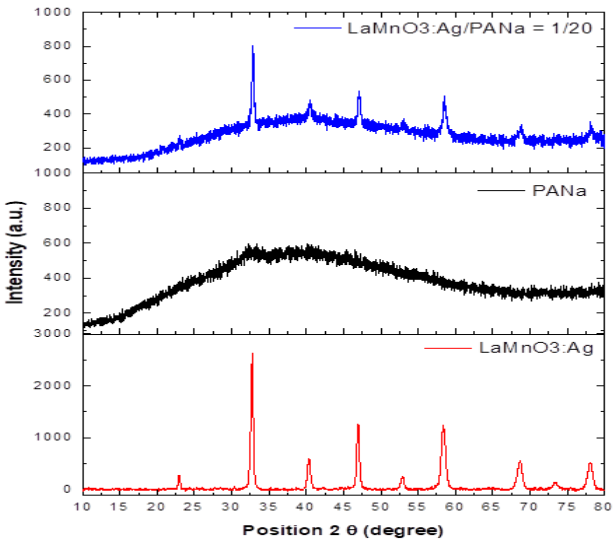

Figure 1. XRD patterns of the studied materials

The structural data for all samples were analyzed by the Rietveld refinement method with FullProf software. According to Markelova et al. [38] the Ag-doped perovskite samples were indexed within the R-3c space group (from $LaMnO_3$:Ag), and the average size of the crystallites was calculated, which was approximately 30 nm [39]. Regarding the structural analysis of the hybrid materials obtained, it can be observed that they present a signature of amorphous content together with a crystalline phase.

3.2. FR-IR Studies

FT-IR spectra of Ag doped perovskite material, sodium polyacrylate, and obtained hybrid material, were recorded in the 4000–400 cm^{-1} range and the results are presented in Figure 2. The broad bands with the maximum around 3460 cm^{-1}can be assigned to O-H stretching modes of surface-adsorbed water, due to the contact of the sample with the environment [40]. In the FTIR spectrum of PANa, the broad band specific to the vibration of the OH group (3361 cm^{-1}) can be observed. The intense peak at 1651 cm^{-1} corresponds to C-OH deformation vibrations, 2948 cm^{-1} corresponds to nCH and nCH2 vibrations in the polymer structure and the two bands at

1427 cm^{-1} and 1273 cm^{-1} are characteristic of carboxylic acid salts (symmetric stretching vibrations of carboxyl anions -COO−). The major functional groups of host polymer can be found in the spectrum of the hybrid material. The FT-IR spectrum of the hybrid material shows certain differences regarding the position of the absorption bands corresponding to PANa and variations of intensities.

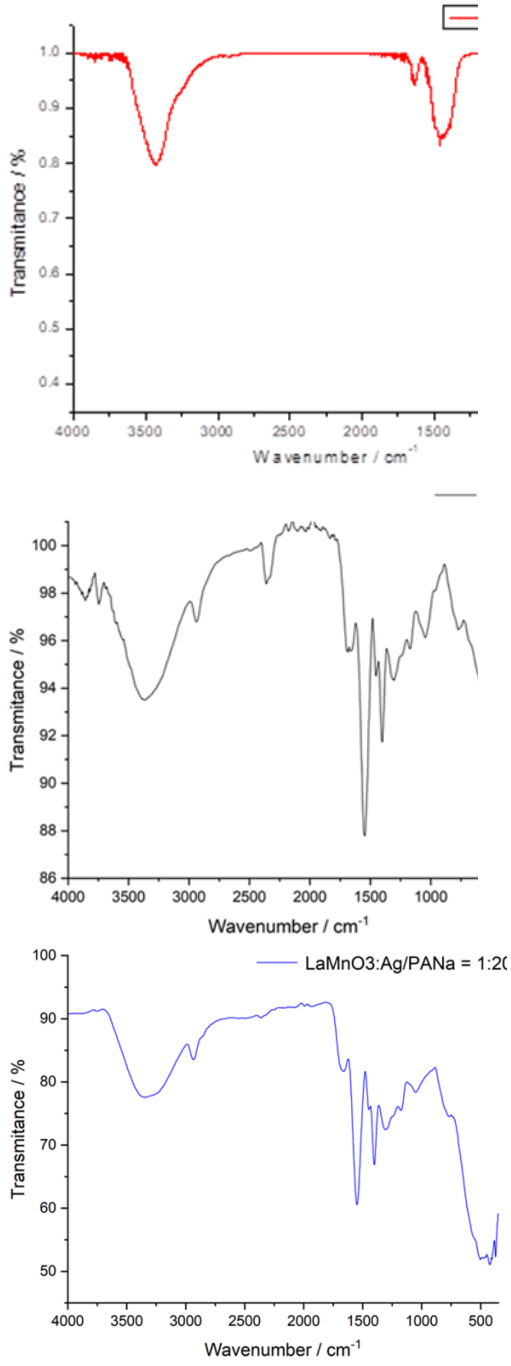

Figure 2. FTIR spectra of the of the studied materials

The strong peak observed at ~1400 cm^{-1} and 1500 cm^{-1} are the symmetrical stretching vibration and asymmetric stretching vibration of C=O in the carboxylate, which is observed in PANa and PANa-$LaMnO_3$:Ag [41].

3.3. Raman Analysis

Specific peaks for $LaMnO_3$ are expected to be present in the region 485-490 cm^{-1}, 646-651 cm^{-1} and 350-374 cm^{-1} corresponding to the stretching modes of Mn-O bond [42]. The addition of PANa (sodium polyacrylate) increased the intensity of peaks; still the specific $LaMnO_3$ bands are not very visible in the presence of Ag, suggesting that the Ag may lessen the clarity of the bands. As a rule, regarding the adsorption of molecules on metal surface, those molecular vibrations that are in parallel position to the surface exhibit weakened spectra bands [43]. Other factor may be the size of the Ag, whereas the bigger size increases the intensity of the bands, respectively lessens the intensity in the presence of smaller Ag size [44]. In addition, the intensity of present bands may also be influenced by the number of Ag atoms that are connected to the material [45]. However, sodium polyacrylate specific bands are visible and in accordance with the specialized literature.

The carbonyl stretching vibration specific to the carboxylic group is observed around 1700 cm^{-1} together with the carboxylate group (-COO-) stretching vibration located at 1605 cm^{-1} [46, 47]. Several strain vibrations were also observed, specifically the CH_2 strains (1463 cm^{-1}), the CH_2 group strains in the polyacrylate backbone (1416 cm^{-1}) and the CH group strains in the carbonyl bonds (1335 cm^{-1}) [46, 48]. The out-of-plane bending of OH corresponding to C-COOH and C-COO- were also observed at 903 cm^{-1} and 864 cm^{-1} respectively [46].

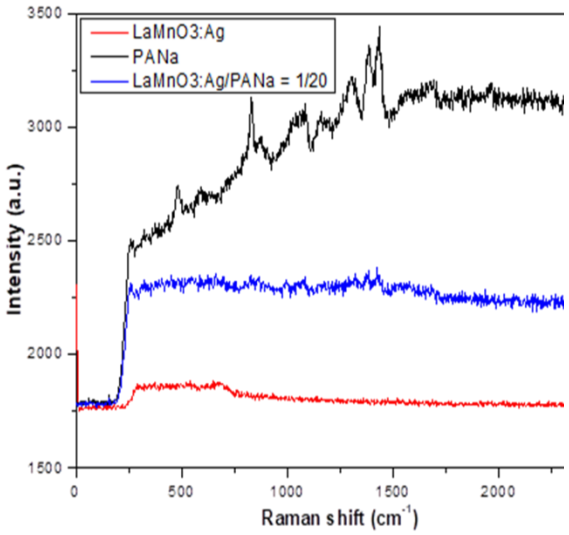

Figure 3. Raman spectra of studied materials

The ratio of water to sodium polyacrylate and other contents influences the results of the Raman spectra, revealing the importance of content ratio of the material. It is known that any change in the content of the material can cause structural changes. According to Di Maggio et al. [46] the changes are more visible in their case, mainly because the materials analyzed were in the form of gels, while in our study the materials are dry and also contain $LaMnO_3$. Therefore, it was observed that the bands around 865 cm^{-1} tend to decrease in combination with $LaMnO_3$ due to C-C bond stretching specific to the C-COO- group. The same situation is observed for the band located at 903 cm^{-1} specific for C-COOH which also weakens. The lower intensity also occurs in the case of bands around 1335 cm^{-1}, followed by 1417 cm^{-1} and 1466 cm^{-1}.

3.4. SEM investigations

In order to carry out a comparative study, both for the perovskite and polymer materials, as well as for the obtained hybrid materials, the surface morphology and the elemental composition were made. The studied materials were analyzed in the low vacuum working mode, at an acceleration voltage of 30 kV, using the LFD detector. Thus, the qualitative and quantitative results are presented in Figure 4.

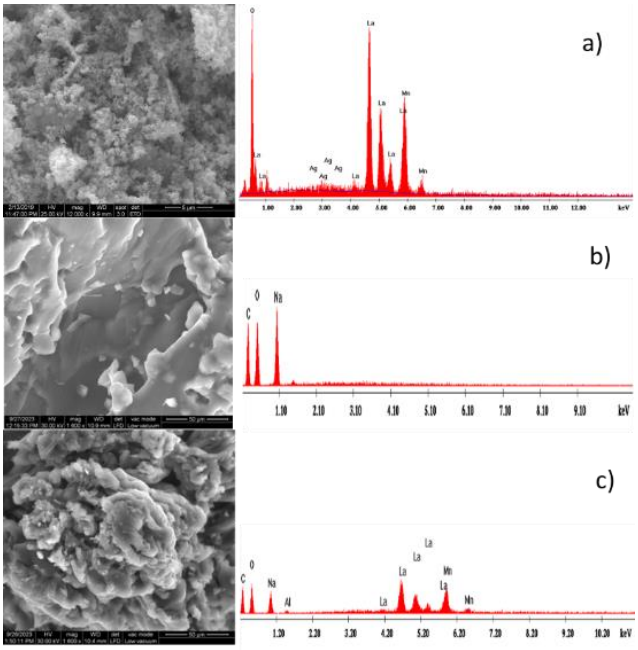

Figure 4. SEM images and EDX spectra of the studied materials:
a) LaMnO3:Ag; b) PANa; c) $LaMnO_3$:Ag/PANa

4. Conclusions

This paper reports for the first time obtaining through wet trituration method at ambient temperature and morpho-structural characterization of materials based on perovskite doped with Ag, functionalized with sodium polyacrylate. In future studies, these materials will be tested in order to use them as a sensitive layer for obtaining detection sensors with applications in food industry.

Acknowledgements

This work was supported by the POC/1025/1/3, Cod SMIS 2014+ 156350.

References

1. Mathew, N.P.; Kumar, N.R.; Radhakrishnan, R., First principle study of the structural and optoelectronic properties of direct bandgap double perovskite $Cs_2AgInCl_6$, *Materials Today: Proceedings* **2020**, *33*, 1252–1256.
2. Huang, H.; Pradhan, B.; Hofkens, J.; Roeffaers, M.B.J.; Steele, J.A., Solar-driven metal halide perovskite photocatalysis: design, stability, and performance, *ACS Energy Letters* **2020**, *5*, 1107–1123.

3. Das, N.; Kandimalla, S., Application of perovskites towards remediation of environmental pollutants: an overview: a review on remediation of environmental pollutants using perovskites, *International Journal of Environmental Science and Technology* **2017**, *14*, 1559–1572.
4. Eskandari, N.; Nabiyouni, G.; Masoumi, S.; Ghanbari, D., Preparation of a new magnetic and photo-catalyst $CoFe_2O_4$–$SrTiO_3$ perovskite nanocomposite for photo-degradation of toxic dyes under short time visible irradiation, Composites *Part B: Engineering* **2019**, *176*, 107343.
5. Petrovi, M.; Chellappan, V.; Ramakrishna, S., Perovskites: solar cells & engineering applications – materials and device developments, *Solar Energy* **2015**, *122*, 678–699.
6. Adjokatse, S.; Fang, H.-H.; Loi, M.A., Broadly tunable metal halide perovskites for solid-state light-emission applications, *Materials Today* **2017**, *20*, 413–424.
7. Zhou, Y.; Chen, J.; Bakr, O.M.; Mohammed O.F., Metal halide perovskites for X-ray imaging scintillators and detectors, *ACS Energy Letters* **2021**, *6*, 739–768.
8. Dandia, A.; Saini, P.; Sharma, R.; Parewa, V., Visible light driven perovskite-based photocatalysts: A new candidate for green organic synthesis by photochemical protocol, *Current Research in Green and Sustainable Chemistry* **2020**, *3*, 100031.
9. Nketia-Yawson, V.; Shim, J.W.; Nketia-Yawson, B.; Jo, J.W., Surface functionalized electrolyte-gated perovskite transistors with enhanced performance via insulating polymer additive, *Applied Surface Science* **2023**, *640*, 158297.
10. Kavitha, M.; Sakorikar, T.; Vayalamkuzhi, P.; Jaiswal, M., Breakdown of water super-permeation in electrically insulating graphene oxide films: role of dual interlayer spacing, *Nanotechnology* **2018**, *29*, 325706.
11. Messegee Z., Mamun A.A., Ava T.T., Namkoong G., Abdel-Fattah T.M., Characterization of Perovskite ($CH_3NH_3PbI_3$) Degradation with the Integration of Different Polymers for Increased Stability, *Materials Letters* **2019**, *236*, 159-162.
12. Thien, G.S.H.; Chan, K.-Y.; Marlinda, A.R.; Sarjidan, M.A.M.; Majid W.H.A.; Yap B.K., Active polymer-based halide perovskites for light-driven applications: A review, *Applied Surface Science Advances* **2024**, *19*, 100538
13. Karami, M.; Ghanbari, M.; Amiri, O.; Salavati-Niasari, M., Enhanced antibacterial activity and photocatalytic degradation of organic dyes under visible light using cesium lead iodide perovskite nanostructures prepared by hydrothermal method, *Separation and Purification Technology* **2020**, *253*, 117526.
14. Niu, B.; Wu, H.; Yin, J.; Wang, B.; Wu, G.; Kong, X.; Yan, B.; Yao, J.; Li, C.Z., Chen H., Mitigating the lead leakage of high-performance perovskite solar cells via in situ polymerized networks, *ACS Energy Letters* **2021**, *6*, 3443–3449.
15. Zhang, M.; Zhang, F.; Shi, K.; Zhang, W.; Huang, J.; Qiu, H., Polymer passivation of defects in inorganic perovskite solar cells, *Optoelectronics Letters* **2022**, *18*, 338–342.
16. Bkkar, M.; Olekhnovich, R.; Kremleva, A.; Sitnikova, V.; Kovach, Y.; Zverkov, N.; Uspenskaya, M., Influence of electrospinning setup parameters on properties of polymer-perovskite nanofibers, *Polymers* **2023**, *15*, 731.
17. Chowdhury, T.H.; Reo, Y.; Yusoff, A.R.B.M.; Noh, Y.-Y., Sn-based perovskite halides for electronic devices, *Advanced Science* **2022**, *9*, 2203749.
18. Liu, Q.; Gao, S.; Xu, L.; Yue, W.; Zhang, C.; Kan, H.; Li, Y.; Shen, G., Nanostructured perovskites for nonvolatile memory devices, *Chemical Society Reviews* **2022**, *51*, 3341–3379.
19. Na, H.; Li, M.Q.; Cha, J.; Kim, S.; Jin, H.; Baek, D.; Kim, M.K.; Sim, S.; Lee, M.; Kim, M.; Lim, J.; Lee, J.; Kim, M., Passivating detrimental grain boundaries in perovskite films with strongly interacting polymer for achieving high-efficiency and stable perovskite solar cells, *Applied Surface Science* **2023**, *626*, 157209.
20. Wang S.; Li M.; Song C.; Zheng C.; Li J.; Li Z.; Zhang Y.; Yao J.; Phenethylammonium iodide modulated SnO_2 electron selective layer for high performance, self-powered metal halide perovskite photodetector, *Applied Surface Science* **2023**, *623*, 156983.
21. Căta, A.; Țăranu, B.-O.; Ienașcu, I.M.C.; Sfîrloagă, P., New PVP–Ag or Pd-Doped Perovskite Oxide Hybrid Structures for Water Splitting Electrocatalysis, *Applied Sciences* **2024**, *14*, 1186.
22. Tachibana, S.; Wang, W.F.; Sekine, T.; Takeda, Y.; Hong, J.; Yoshida, A.; Abe, M.; Miura, R.; Watanabe, Y.; Kumaki, D.; Tokito, S., A printed flexible humidity sensor with high sensitivity and fast response using a cellulose nanofiber/carbon black composite, *ACS Applied*

Materials & Interfaces **2022**, *14*, 5721–5728.
23. Zhang, Z.; Li, F.; Zheng, Y., Highly sensitive resistive humidity sensor based on strontium-doped lanthanum ferrite nanofibers, *Sensors & Actuators, B: Chemical* **2023**, *358*, 114435.
24. Vasileva, F.; Popov, V.; Antonova, I.; Smagulova, S., Screen-printed structures from a highly conductive mildly oxidized graphene suspension for flexible electronics, *Materials* **2022**, *15*, 1256.
25. Gong, L.K.; Wang, X.W.; Zhang, D.Z.; Ma, X.D.; Yu, S.J., Flexible wearable humidity sensor based on cerium oxide/graphitic carbon nitride nanocomposite self-powered by motion-driven alternator and its application for human physiological detection, *Journal of Materials Chemistry A* **2021**, *9*, 5619–5629.
26. Guo, C.Y.; Dong, X.; Zhang, X.F.; Cheng, X.L.; Li, Q.; Sun, Y.J.; Liu, W.; Huo, L.H.; Xu, Y.M., Controllable construction of Ho_2O_3 nanomaterials with different dimensions (1D, 2D, and 3D) for real-time monitoring human breathing and body surface humidity detection, *Materials Chemistry A* **2021**, *9*, 11632 -11640.
27. Liu, H.T.; Song, X.D.; Wang, X.Y.; Wang, S.H.; Yao, N.; Li, X.; Fang, W.; Tong, L.M.; Zhang, L., Optical microfibers for sensing proximity and contact in human-machine interfaces, *ACS Applied Materials & Interfaces* **2022**, *14*, 14447–14454.
28. Qi, P.J.; Xu, Z.W.; Zhou, T.T.; Zhang, T.; Zhao, H.R., Study on a quartz crystal microbalance sensor based on chitosan-functionalized mesoporous silica for humidity detection, *Journal of Colloid and Interface Science* **2021**, *583*, 340–350.
29. Guo, C.Y.; Xin, Y.Y.; Liu, Y.; Na, B.Y.; Meng, W.Q.; Zhang, X.F.; Cheng, X.L.; Huo, L.H.; Wang, T.T.; Xu, Y.M., Noncontact sensing for water area scanning identification based on Ho_2O_3/GO humidity sensor, *Sensors & Actuators, B: Chemical* **2023**, *385*, 133683.
30. Wang, D.Y.; Zhang, D.Z.; Li, P.; Yang, Z.M.; Mi, Q.; Yu, L.D., Electrospinning of flexible poly(vinyl alcohol)/MXene nanofiber-based humidity sensor self-powered by monolayer molybdenum diselenide piezoelectric nanogenerator, *Micro & Nano Letters* **2021**, *13*, 57.
31. Qi, R.R.; Lin, X.Z.; Dai, J.X.; Zhao, H.R.; Liu, S.; Fei, T.; Zhang, T., Humidity sensors based on MCM-41/polypyrrole hybrid film via in-situ polymerization, *Sensors & Actuators, B: Chemical* **2018**, *277*, 584–590.
32. Zhang, K.; Hu, R.F.; Fan, G.K.; Li, G., Graphene oxide/chitosan nanocomposite coated quartz crystal microbalance sensor for detection of amine vapors, *Sensors & Actuators, B: Chemical* **2017**, *243*, 721–730.
33. Gosden, D.; Studley, M.; Rossiter, J., Material extrusion of sodium polyacrylate superabsorbent polymer, *Additive Manufacturing* **2023**, *78*, 103886.
34. Dai J.X., Zhao H.R., Lin X.Z., Liu S., Fei T., Zhang T., Design strategy for ultrafast-response humidity sensors based on gel polymer electrolytes and application for detecting respiration, *Sensors & Actuators, B: Chemical* **2020**, *304*, 127270.
35. Ponzoni, C.; Cannio, M.; Rosa, R.; Leonelli, C., Stabilization of bismuth ferrite suspensions in aqueous medium with sodium polyacrylate characterized by different molecular weights, *Materials Chemistry and Physics* **2015**, *149–150*, 246-253**.**
36. Zhang, Z.; Lin, Y.; Liu, F., Preparation, crystallization and properties of $Bi2WO_6$ nanoparticle, *Colloids and Surfaces A: Physicochemical and Engineering Aspect*s **2020**, *590*, 124493.
37. Sfirloaga, P.; Poienar, M.; Malaescu, I.; Lungu, A.; Vlazan, P., Perovskite type lanthanum manganite: Morpho-structural analysis and electrical investigations, *Rare Earth* **2018**, *36*, 499–504.
38. Markelova, M.N.; Kotova, O.V.; Kaul, A.R., Magnetic luminescent material based on silver doped lanthanum manganite and euro-pium salts with 1,10-phenanthroline, *Russian Chemical Bulletin* **2015**, *64*, 219–223.
39. Sfirloaga, P.; Vlase, G.; Vlase, T.; Malaescu, I.; Marin, C.N.; Vlazan, P., Silver doping in lanthanum manganite materials: structural and electrical properties, *Journal of Thermal Analysis and Calorimetry* **2020**, *142*, 1817-1823.
40. Sfirloaga, P.; Ivanovici, M.-G.; Poienar, M.; Ianasi, C.; Vlazan, P., Investigation of Catalytic and Photocatalytic Degradation of Methyl Orange Using Doped $LaMnO_3$ Compounds, *Processes* **2022**, *10*, 2688.
41. Tan, M.J.; Li, B.; Chee, P.; Ge, X.; Liu, Z.; Zong, Y.; Loh, X.J., Acrylamide-derived freestanding polymer gel electrolyte for flexible metal-air batteries, *Journal of Power Sources* **2018**, *400*, 566-571.

42. Martin-Carron, L.; de Andrés, A., Melting of the cooperative Jahn-Teller distortion in LaMnO3 single crystal studied by Raman spectroscopy, *The European Physical Journal B* **2001**, *22*, 11-16.
43. Mao, H.; Feng, J.; Ma, X.; Wu, C.; Zhao, X., One-dimensional silver nanowires synthesized by self-seeding polyol process, *Journal of Nanoparticle Research* **2012**, *14*, 887.
44. Kim, K.; Choi, J.-Y.; Lee, H.B.; Shin, K.S., Raman scattering of 4-aminobenzenethiol sandwiched between Ag nanoparticle and macroscopically smooth Au substrate: Effects of size of Ag nanoparticles and the excitation wavelength, *The Journal of Chemical Physic*s **2011**, *135*, 124705.
45. Wan, F.; Shi, H.; Chen, W.; Gu, Z.; Du, L.; Wang, P.; Wang, J.; Huang, Y., Charge Transfer Effect on Raman and Surface Enhanced Raman Spectroscopy of Furfural Molecules, *Nanomaterials* **2017**, *7*(8), 210.
46. Di Maggio, R.; Dirè, S.; Callone, E.; Bergamonti, L.; Lottici, P.P.; Albatici, R.; Rigon, R.; Ataollahi, N., Super-adsorbent polyacrylate under swelling in water for passive solar control of building envelope, *SN Applied Sciences* **2020**, *2*, 45.
47. Grabowska, B.; Sitarz, M.; Olejnik, E.; Kaczmarska, K.; Tyliszczak, B., FT-IR and FT-Raman studies of cross-linking processes with Ca2+ ions, glutaraldehyde and microwave radiation for polymer composition of poly(acrylic acid)/sodium salt of carboxymethyl starch – In moulding sands, Part II, *Spectrochimica Acta Part A: Molecular and Biomolecular Spectroscopy* **2015**, *151*, 27–33.
48. Dong, J.; Ozaki, Y.; Nakashima, K., Infrared, Raman, and Near-Infrared Spectroscopic Evidence for the Coexistence of Various Hydrogen-Bond Forms in Poly(acrylic acid), *Macromolecules* **1997**, *30*, 1111–1117.